Experimental test of Leggett's inequalities with solid-state spins

Xianzhi Huang,* Xiaolong Ouyang,* Wenqian Lian,* Wengang Zhang, Xin Wang, Huili Zhang, Yefei Yu, Li He, Yanqing Liu, Xiuying Chang, Dong-Ling Deng,† and Luming Duan‡

Center for Quantum Information, IIIS, Tsinghua University, Beijing 100084, People's Republic of China

(Received 21 December 2019; accepted 15 June 2020; published 9 July 2020)

Bell's theorem states that no local hidden-variable model is compatible with quantum mechanics. Surprisingly, even if we release the locality constraint, certain nonlocal hidden-variable models, such as the one proposed by Leggett, may still be at variance with the predictions of quantum physics. Here, we report an experimental test of Leggett's nonlocal model with solid-state spins in a diamond nitrogen-vacancy center. We entangle an electron spin with a surrounding weakly coupled ^{13}C nuclear spin and observe that the entangled states violate Leggett-type inequalities by more than four and seven standard deviations for six and eight measurement settings, respectively. Our experimental results are in full agreement with quantum predictions and violate Leggett's nonlocal hidden-variable inequality with a high level of confidence.

DOI: 10.1103/PhysRevA.102.012210

I. INTRODUCTION

Realism and locality are two fundamental concepts in classical physics [1–3]. Roughly speaking, locality requires that events that happened in spacelike separated regions cannot influence each other, while realism suggests that the results of observations are predetermined by the intrinsic properties of a physical system and should be independent of the measurement [4]. Quantum physics, however, challenges these concepts in a profound way—no hidden-variable theory based on the joint assumption of realism and locality can reproduce all quantum correlations [2,3]. This fact is now well known through Bell's theorem [5] and has been verified by a number of experiments with different platforms [6–23]. In particular, recent experiments with entangled electron spins [19], photons [20,21], and atoms [22] have been reported to close the detection and locality loophole simultaneously. This, together with the Bell Test project that attempts to close the freedom-of-choice loophole [24], has reasonably established that the violation of local realism in quantum physics is a validated fact.

Then, should nonlocal realism be consistent with quantum physics? This is a natural question, but the answer is complicated. On the one hand, Bohm's interpretation [25] of quantum mechanics clearly implies that certain nonlocal hidden-variable (NLHV) models can indeed reproduce all predictions of quantum physics. On the other hand, however, there also exist other NLHV models that are proved to be incompatible with quantum predictions. The first testable example of such NLHV model was the one proposed by Suarez and Scarani [26], which has been falsified in a series of subsequent experiments [27,28]. Another notable example involves the one introduced by Leggett [29]. This NLHV model fulfills the so-called Leggett's inequalities, but quantum correlations can violate them. Leggett's model has attracted considerable attention in the community [30–41] and a number of experiments have been carried out to test it [30–38,42]. All these experiments support the predictions of quantum mechanics and show violations of Leggett's inequalities. Nevertheless, most of these experiments use photons [30–37]; here, Leggett's model is instead tested in a solid-state system. Given the important roles that solid-state systems play in quantum information sciences, it is highly desirable that the Leggett inequalities should also be tested in such systems. Violation of Leggett's inequality requires preparation of entangled states with a very high fidelity and correlation measurements in various complementary settings, which are experimentally challenging. Therefore, the test of Leggett's inequality, apart from its fundamental interest, is also a demonstration of good quality of entanglement control in the corresponding quantum systems. In addition, violation of NLHV models implies the intrinsic random properties of quantum mechanics, which might also be explored to build random number generators which can generate true random numbers [43,44]. A demonstration of violations of Leggett's inequality in solid-state systems would be useful to construct random number generators in practical applications.

In this paper, we fill this important gap by reporting an experimental test of Leggett's NLHV model with solid-state spins in a diamond nitrogen-vacancy center (see Fig. 1 for a pictorial illustration). Following Branciard *et al.* [33], we derive two Leggett-type inequalities with six and eight measurement settings, respectively, without assuming a time ordering of the events as in Leggett's original paper [29]. We entangle an electron spin in the nitrogen-vacancy (NV) center with a surrounding ^{13}C nuclear spin to form a maximally entangled Bell state with high fidelity and perform appropriate single-shot projection measurements on the electron spin to measure the correlations between the electron and nuclear spins. We observe that for large measurement parameter regions, the entangled states violate both the derived six- and eight-setting

*These authors contributed equally to this work.
†dldeng@tsinghua.edu.cn
‡lmduan@tsinghua.edu.cn

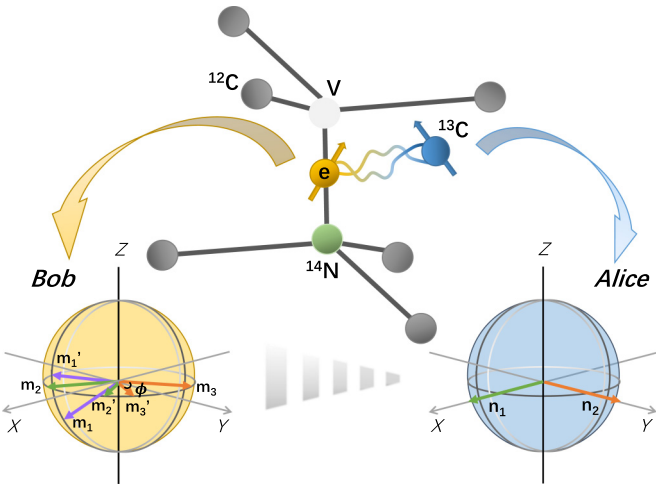

FIG. 1. Tests of Leggett's nonlocal hidden-variable theories with solid-state spins in a diamond nitrogen-vacancy center. An electron spin of the nitrogen-vacancy center is prepared to be entangled with one of its surrounding ^{13}C nuclear spins. We denote the nuclear spin and the electron spin by Alice and Bob, respectively. Measurement settings on the Poincaré sphere are shown for testing Eq. (2).

Leggett-type inequalities. In particular, for the six-setting (eight-setting) inequality, the maximal violation exceeds the classical bound by 4.0 and 10.9 (7.1 and 15.5) standard deviations for the raw data and the data after correction of the readout error, respectively. Our experimental results are in full agreement with quantum predictions and thus falsify Leggett's NLHV model in a solid-state system.

II. LEGGETT'S INEQUALITIES

To begin with, let us first briefly introduce two inequalities based on Leggett's nonlocal model, following a simpler approach introduced by Branciard *et al.* [33]. Consider a common Bell-type experimental scenario: two observers, denoted by Alice and Bob, perform measurements labeled by $\mathbf{n}$ and $\mathbf{m}$ on their qubits, respectively. The outcomes are denoted by α and β ($\alpha, \beta = \pm 1$). For the qubit case, $\mathbf{n}$ and $\mathbf{m}$ are unit vectors on the Poincaré sphere (see Fig. 1 for an illustration) and are independently and freely chosen by Alice and Bob. According to hidden-variable theories [45], the conditional probability distribution $P(\alpha, \beta|\boldsymbol{n}, \boldsymbol{m})$ can be decomposed into a statistical mixture of correlations characterized by the hidden variable λ,

$$P(\alpha, \beta|\boldsymbol{n}, \boldsymbol{m}) = \int_{\Gamma} \rho(\lambda) P_{\lambda}(\alpha, \beta|\boldsymbol{n}, \boldsymbol{m}) d\lambda, \tag{1}$$

where Γ is the total λ space and $\rho(\lambda)$ is a statistical distribution of λ which satisfies $\rho(\lambda) \geqslant 0$ and $\int_{\Gamma} \rho(\lambda) d\lambda = 1$. Strikingly, the constraint of non-negativity of probabilities $P_{\lambda}(\alpha, \beta|\boldsymbol{n}, \boldsymbol{m}) \geqslant 0$ is sufficient to derive testable Leggett-type inequalities which are satisfied by Leggett's NLHV model but can be violated by quantum predictions. The simplest inequality reads (see [33] and Appendix A for details)

$$\mathcal{I}_{26}(\phi) \equiv \left|C_{\mathbf{n}_1,\mathbf{m}_1} + C_{\mathbf{n}_1,\mathbf{m}_1'}\right| + \left|C_{\mathbf{n}_1,\mathbf{m}_2} + C_{\mathbf{n}_1,\mathbf{m}_2'}\right| + \left|C_{\mathbf{n}_2,\mathbf{m}_3} + C_{\mathbf{n}_2,\mathbf{m}_3'}\right| + 2\sin\frac{\phi}{2} \leqslant 6, \tag{2}$$

where $C_{\mathbf{n},\mathbf{m}} = \sum_{\alpha,\beta} \alpha\beta P(\alpha, \beta|\boldsymbol{n}, \boldsymbol{m})$ denotes the usual correlation function and ϕ is the angle between a pair of vectors $\mathbf{m}_i$ and $\mathbf{m}_i'$ ($i = 1, 2, 3$) (see Appendix A). We note that the above inequality is a bit different from the original one introduced in Ref. [33], where three measurement settings for Alice's side were used. Here, we use only two settings for Alice because the tests of this modified inequality are easier to implement in our NV experimental setup.

III. EXPERIMENTAL SETUP AND VIOLATIONS OF LEGGETT'S INEQUALITIES

In the experiment, we use solid-state spins, namely, an electron spin and a surrounding ^{13}C nuclear spin in a diamond NV center [46], to test Leggett-type inequalities. The NV center is a natural doped structure which is composed of a vacancy and an adjacent nitrogen atom that replace the two neighboring carbon atoms [47]. Our experiments utilize the negative charge state of the NV center with an electron spin $S = 1$ (denoted as $|m_s = \pm 1\rangle$ and $|m_s = 0\rangle$) and a nearby weakly coupled ^{13}C nuclear spin $I = 1/2$ (denoted as $|\uparrow\rangle$ and $|\downarrow\rangle$) in a cryostat at temperature around 8 K, with optical initialization and readout achieved through use of resonant transitions [48] between excited states and ground states.

To realize efficient multiqubit control, we need to design a set of single-qubit gates and electron-nuclear two-qubit entangling gates. With a magnetic field B_z aligned along the NV symmetry axis and under the rotating-wave approximation, the effective Hamiltonian of the system in the rotating frame with respect to the modulated electron energy splitting describing the electron spin and a single ^{13}C nuclear spin has the form

$$H_{eff} = A_{zz}\hat{S}_z\hat{I}_z + A_{zx}\hat{S}_z\hat{I}_x + \gamma_n B_z \hat{I}_z, \tag{3}$$

where $\hat{S}_z = \mathrm{diag}\{1, 0, -1\}$ denotes the z component of the spin-one operator, and $\hat{I}_x$ and $\hat{I}_z$ are the Pauli-X and Pauli-Z matrix, respectively (here we define the NV symmetry axis as the z axis); γ_n is the gyromagnetic ratio of the ^{13}C nuclear spin; and A_{zz} and A_{zx} form the parallel and perpendicular components of the hyperfine interaction term between the electron spin and the nuclear spin, with their values determined precisely from previous experiments [49]. Due to the particular mutual interaction, the ^{13}C nuclear-spin processes around the axis conditioned on the electron spin state, so we can construct a set of selective electron-nuclear two-qubit gates based on the dynamical decoupling sequences [50].

One can verify that inequality (2) can be violated in quantum mechanics for a range of ϕ and for various quantum entangled states. The maximal violation is achieved when the left side of Eq. (2) equals $\sqrt{40}$ and this happens at $\phi_0 = 2\arctan\frac{1}{3} \approx 36.9^\circ$ under the maximally entangled singlet state [32]. For this optimally chosen setting, the minimal visibility to observed violation of inequality (2) is about $V_{\min} = 94.3\%$. The minimal visibility measures how much white noise can be added into the Bell state so that the inequality is still violated, i.e., the minimal value of V under the condition that the state $\rho_V = V|\Phi^-\rangle\langle\Phi^-| + (1 - V)\boldsymbol{I}/4$ (here, $\boldsymbol{I}$ is the 4×4 identity matrix) violates inequality (3). The corresponding minimal fidelity is estimated to be $F_{\min} = \sqrt{3V_{\min} + 1}/2 \approx 97.8\%$. This high value of the required

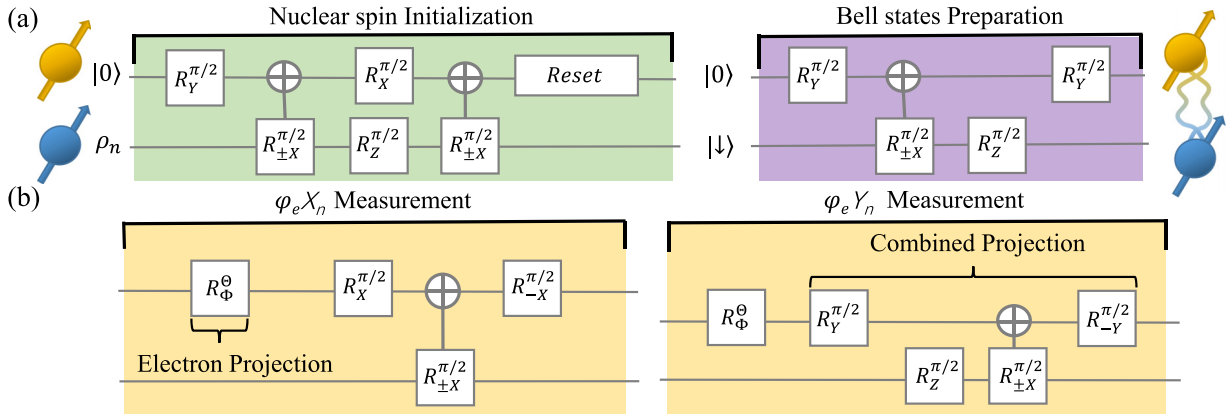

FIG. 2. (a) Experimental sequences for initialization of a weakly coupled ^{13}C nuclear-spin state and preparation of one of the electron-nuclear Bell states. The initial state of the nuclear spin can be flipped by tuning the quantum gate parameters, and the phase settings of two electron microwave π pulses in entanglement preparation can be changed to transform the generation between four Bell states. (b) The measurement sequences for jointly measuring the electron and nuclear spins, in a rotated electron-nuclear basis $\varphi_e X_n/\varphi_e Y_n$. After appropriate basis rotation, the corresponding φ settings' electron spin state is projected to the X_e/Y_e axis and the joint detection can be achieved by following the combined projective optical readout (see Appendix B).

minimum fidelity is a significant challenge for an experimental observation of violation of the Leggett inequality. In our experiments, we have used the dynamical decoupling [50] and optimized the sequence parameters to meet this requirement (see Appendices C–E).

We choose the electron spin to act as the control qubit and the ^{13}C nuclear spin undergoing the conditional rotation as the target qubit. To protect the single nuclear spin from the decoherence effect and avoid the unwanted crosstalk between multiple nuclear spins, we need to optimize the parameters of single and controlled quantum gates based on the precisely characterized hyperfine interaction couplings [49]. The sequence to achieve the nuclear-spin state initialization and electron-nuclear-spin entanglement [51] is shown in Fig. 2(a). First we prepare the electron spin in $|0\rangle$ and, after a swapping procedure [52], the nuclear spin is initialized onto $|\uparrow\rangle$ or $|\downarrow\rangle$ determined by the controlled quantum gate parameters. We then reset the electron spin to be on state $|0\rangle$ and apply the entangling gate on the electron and nuclear spins. After this, the electron and nuclear spins are maximally entangled with the state $|\Phi^-\rangle = (|0_e\uparrow_n\rangle - |1_e\downarrow_n\rangle)/\sqrt{2}$. From the measured expectation values of entanglement witness operators described in Ref. [53], we can obtain a lower bound on the fidelity of our prepared Bell state at 98.2(5)%.

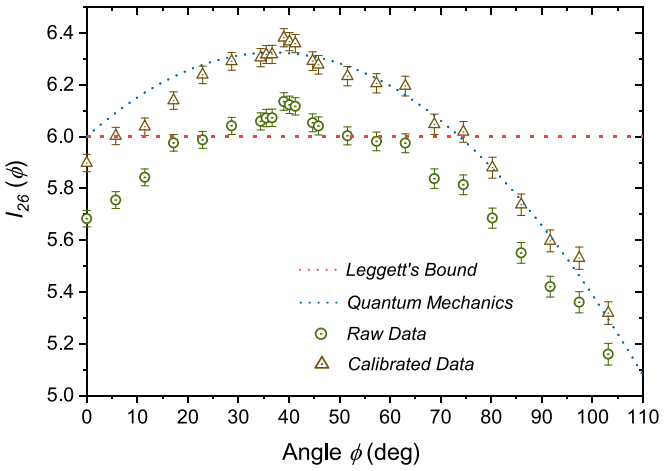

FIG. 3. Experimental violations of the Leggett's inequality with six measurement settings. The dashed orange line indicates the bound of inequality (2), which is satisfied by Leggett's nonlocal hidden-variable model. The dotted line denotes the quantum mechanical prediction and the region above the dashed line implies quantum violation. Our experimental raw data (denoted by circles) of $\mathcal{I}_{26}$ exceed the Leggett's bound for $23.02^\circ < \phi < 51.57^\circ$. The largest violation is observed for $\phi_{\max} = 38.96^\circ$. The triangles show the data after correction of the readout error, and the violating ϕ region in the case becomes broader and the maximal violation also gets bigger. Here, the error bars denote the readout standard deviations.

For the quantum state measurements on the entangled Bell state, instead of measuring electron spin and nuclear spin separately [54], we choose appropriate basis projections of both electron and nuclear spin followed by Z-basis optical measurement to read out the electron-nuclear-spin state simultaneously in a single-shot readout scheme with sufficient average fidelity at cryogenic temperature [Fig. 2(b)]. The specific process starts with the rotation of electron spin from pairs $(\boldsymbol{m_i}, \boldsymbol{m_i'})$, which satisfy the corresponding φ settings to the X_e/Y_e basis of the two-qubit system, followed by a joint measurement of X_eX_n/Y_eY_n using the particularly designed sequence (see Appendix E for the details). In this way, we are able to measure the desired correlations appearing in Eq. (2).

We vary the measurement angle parameter ϕ in a discrete way and, for each value of ϕ, we measure the quantum expectation value of $\mathcal{I}_{26}$. Our experimental results are shown in Fig. 3. From this figure, our experimental results match the theoretical predictions qualitatively and the Leggett's inequality (2) is violated for $23.02^\circ < \phi < 51.57^\circ$. The largest violation occurs at $\phi_{\max} = 38.96^\circ$ and the violation for the experimental raw data is 6.136 ± 0.034, violating Eq. (2) by more than four standard deviations. In addition, since in our experiments the state initialization and projective readout procedures consist of the same number of similar gate operations, we can follow a standard recipe, as in Ref. [54], to correct the readout error (see, also, Appendix F for the details). After

this correction, each measured correlation will be closer to its corresponding theoretical prediction without experimental imperfections and the violation of the Leggett's inequality will be further enhanced. Our experimental data after the readout error correction are also shown in Fig. 3. It is clear from this figure that after the readout error correction, our experimental results have excellent agreement with the theoretical quantum predictions, and the the maximal violation in this case is 6.382 ± 0.035, which violates Eq. (2) by more than 10.9 standard deviations.

To obtain stronger quantum violations, one can increase the number of measurement settings, similar to the case of testing Bell inequalities. In Eq. (2), Alice has two measurement settings and Bob has six settings. Following a similar derivation, we obtain another Leggett-type inequality, where Bob has eight measurement settings (see Appendix A),

$$\begin{aligned}\mathcal{I}_{28}(\varphi) \equiv & \left|C_{\mathbf{n}_1,\mathbf{m}_1} + C_{\mathbf{n}_1,\mathbf{m}_1'}\right| + \left|C_{\mathbf{n}_1,\mathbf{m}_2} + C_{\mathbf{n}_1,\mathbf{m}_2'}\right| \\ & + \left|C_{\mathbf{n}_2,\mathbf{m}_3} + C_{\mathbf{n}_2,\mathbf{m}_3'}\right| + \left|C_{\mathbf{n}_2,\mathbf{m}_4} + C_{\mathbf{n}_2,\mathbf{m}_4'}\right| \\ & + \frac{8}{\sqrt{6}} \sin\frac{\varphi}{2} \leqslant 8. \end{aligned} \tag{4}$$

It is straightforward to check that inequality (4) is violated in quantum physics for a large range of φ, with measurement settings shown in Fig. 4(a), and the maximal violation occurs at $\varphi_0 = \pi - 2\arctan\sqrt{\frac{6}{7}} \approx 44.4^\circ$. The maximal violation of inequality (4) is $8\sqrt{\frac{7}{6}}$ and the threshold visibility is $V_{\min} \approx 91.3\%$ with the corresponding threshold fidelity $F_{\min} = 96.7\%$, which are both smaller than the ones for the six-setting Eq. (2). Our experimental results for testing Eq. (4) are plotted in Fig. 4(b), from which it is evident that the inequality is violated for $17.96^\circ < \varphi < 71.34^\circ$. The maximal violation is 8.323 ± 0.045, occurring at $\varphi_{\max} = 40.11^\circ$, which violates Eq. (4) by more than 7.1 standard deviations. With readout error correction, the maximal violation is 8.729 ± 0.047 (see Appendix F), violating Eq. (4) by more than 15.5 standard deviations. Our experiments confirm that the violation of the eight-setting inequality (4) is notably larger than that of the six-setting inequality (2).

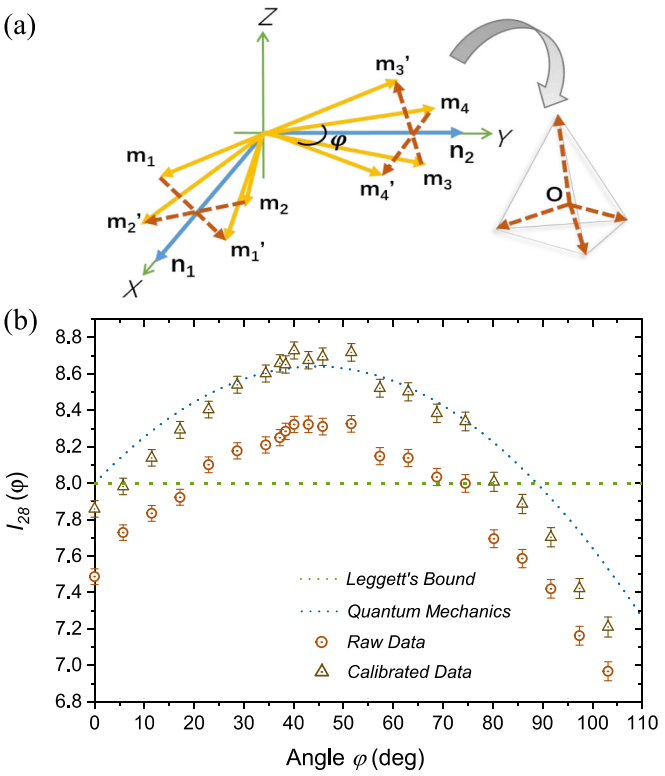

FIG. 4. (a) Measurement settings for nuclear (blue arrows) and electron (yellow arrows) spins on the Poincaré sphere for testing Eq. (4) (see Appendix E). The four vectors $\{\vec{e}_i = \boldsymbol{m}_i - \boldsymbol{m}_i'\}$ point to the four vertices of the regular tetrahedron. (b) Experimental violations of the Leggett's inequality (4). The quantum expectation of $\mathcal{I}_{28}$ exceeds the Leggett's bound for $17.96^\circ < \varphi < 71.34^\circ$ and the maximal violation occurs at $\varphi_{\max} = 40.11^\circ$ for the raw data (circle). With readout correction, we get the broader violating ϕ region and the bigger maximal violation (triangle).

IV. CONCLUSION

In summary, we have experimentally tested Leggett's NLHV model in a solid-state system. Our experimental results are in agreement with quantum predictions and show clear violation of the Leggett-type inequalities with a high confidence level, thus falsifying Leggett's model with solid-state spins. Our discussion is mainly focused on the two-qubit case, but its generalizations to multiple qubits are possible and worth future investigations. In addition, it would be interesting to experimentally test nonlocal causality [55] with solid-state spins in a similar setup.

ACKNOWLEDGMENTS

This work was supported by the Frontier Science Center for Quantum Information of the Ministry of Education of China, Tsinghua University Initiative Scientific Research Program, and the National Key Research and Development Program of China (Grant No. 2016YFA0301902).

APPENDIX A: DERIVATION OF THE LEGGETT'S INEQUALITIES

In this Appendix, we give more details on how to derive the two Leggett's inequalities used in the main text, following Ref. [33]. We consider a common Bell-type experimental scenario, where two observers, denoted by Alice (A) and Bob (B), perform measurements labeled by **n** and **m** on their qubits, respectively. Their outcomes are denoted by α and β ($\alpha, \beta = \pm 1$). From the hidden-variable theories, the conditional probability distribution $P(\alpha, \beta|\boldsymbol{n}, \boldsymbol{m})$ can be decomposed into a statistical mixture of correlations characterized by the hidden variable λ,

$$P(\alpha, \beta|\boldsymbol{n}, \boldsymbol{m}) = \int_\Gamma \rho(\lambda) P_\lambda(\alpha, \beta|\boldsymbol{n}, \boldsymbol{m}) d\lambda, \tag{A1}$$

where Γ denotes the total hidden-variable space and $\rho(\lambda)$ is a statistical distribution of λ, satisfying $\rho(\lambda) \geqslant 0$ and $\int_\Gamma \rho(\lambda) d\lambda = 1$. As discussed in Ref. [33], in the qubit case,

one can write the above correlations as

$$P(\alpha,\beta|\boldsymbol{n},\boldsymbol{m}) = \tfrac{1}{4}[1+\alpha\mathcal{L}_\lambda^A(\boldsymbol{n},\boldsymbol{m})+\beta\mathcal{L}_\lambda^B(\boldsymbol{n},\boldsymbol{m}) + \alpha\beta\mathcal{L}_\lambda^{AB}(\boldsymbol{n},\boldsymbol{m})]. \tag{A2}$$

One advantage of this expression is that it enables one to clearly distinguish the marginals and the correlation coefficient, as discussed in Ref. [33]. For instance, Alice and Bob's marginal can be, respectively, expressed as

$$\mathcal{L}_\lambda^A(\boldsymbol{n},\boldsymbol{m}) = \sum_{\alpha,\beta}\alpha P_\lambda(\alpha,\beta|\boldsymbol{n},\boldsymbol{m}), \tag{A3}$$

$$\mathcal{L}_\lambda^B(\boldsymbol{n},\boldsymbol{m}) = \sum_{\alpha,\beta}\beta P_\lambda(\alpha,\beta|\boldsymbol{n},\boldsymbol{m}). \tag{A4}$$

Similarly, the two-qubit correlation coefficients read

$$\mathcal{L}_\lambda^{AB}(\boldsymbol{n},\boldsymbol{m}) = \sum_{\alpha,\beta}\alpha\beta P_\lambda(\alpha,\beta|\boldsymbol{n},\boldsymbol{m}). \tag{A5}$$

In fact, from the above inequalities [Eqs. (A3) and (A4)], it is obvious that $\mathcal{L}_\lambda^A(\boldsymbol{n},\boldsymbol{m})$ and $\mathcal{L}_\lambda^B(\boldsymbol{n},\boldsymbol{m})$ have their physical meaning of the average. Taking $\mathcal{L}_\lambda^{AB}(\boldsymbol{n},\boldsymbol{m})$, for example, it stands for the average value of the product $\alpha\beta$ when the hidden variable is specified by λ, and Alice and Bob perform their measurements $\mathbf{n}$ and $\mathbf{m}$, respectively. Moreover, as in Ref. [33], we also only concentrate on correlations satisfying the so-called no-signaling condition, which implies the independence of marginals on the other observer's inputs. Here, it indicates the following two equations:

$$\mathcal{L}_\lambda^A(\boldsymbol{n},\boldsymbol{m}) = \mathcal{L}_\lambda^A(\boldsymbol{n}), \quad \mathcal{L}_\lambda^B(\boldsymbol{n},\boldsymbol{m}) = \mathcal{L}_\lambda^B(\boldsymbol{m}). \tag{A6}$$

The probability distributions $P_\lambda(\alpha,\beta|\boldsymbol{n},\boldsymbol{m})$ should be nonnegative. This implies four inequalities:

$$1+\mathcal{L}_\lambda^A+\mathcal{L}_\lambda^B+\mathcal{L}_\lambda^{AB} \geqslant 0, \tag{A7a}$$

$$1+\mathcal{L}_\lambda^A-\mathcal{L}_\lambda^B-\mathcal{L}_\lambda^{AB} \geqslant 0, \tag{A7b}$$

$$1-\mathcal{L}_\lambda^A+\mathcal{L}_\lambda^B-\mathcal{L}_\lambda^{AB} \geqslant 0, \tag{A7c}$$

$$1-\mathcal{L}_\lambda^A-\mathcal{L}_\lambda^B+\mathcal{L}_\lambda^{AB} \geqslant 0. \tag{A7d}$$

Leggett's original idea is mainly based on pairs of photons. To derive the Leggett-type inequality, there are three basic assumptions: (i) Realism. All measurement outcomes are predetermined and independent of the measurement. (ii) Perfect polarization. Each photon in the pairs is perfectly polarized. (iii) Malus' law. Local marginals should obey Malus's law.

From Eqs. (A7a)–(A7d), it is easy to obtain

$$\left|\mathcal{L}_\lambda^A(\boldsymbol{n}) \pm \mathcal{L}_\lambda^B(\boldsymbol{m})\right| \leqslant 1 \pm \mathcal{L}_\lambda^{AB}(\boldsymbol{n},\boldsymbol{m}). \tag{A8}$$

Consider one measurement setting $\boldsymbol{n}$ for Alice and two measurement settings $\boldsymbol{m},\boldsymbol{m}'$ for Bob. Then, by using inequalities (A7a)–(A7d) and the triangle inequality, one obtains

$$\left|\mathcal{L}_\lambda^{AB}(\boldsymbol{n},\boldsymbol{m}) \pm \mathcal{L}_\lambda^{AB}(\boldsymbol{n},\boldsymbol{m}')\right| + \left|\mathcal{L}_\lambda^B(\boldsymbol{m}) \mp \mathcal{L}_\lambda^B(\boldsymbol{m}')\right| \leqslant 2. \tag{A9}$$

As argued in Ref. [33], Leggett's model has a basic assumption that locally everything happens as if each single quantum system would always be in a pure state. Consequently, we may assume the hidden variables λ can be denoted by normalized vectors $\mathbf{u}$, $\mathbf{v}$ on the Poincaré sphere,

$$\lambda = |\boldsymbol{u}\otimes\boldsymbol{v}\rangle, \tag{A10}$$

and the local marginals should obey (a condition similar to the Malus' law for photons)

$$\mathcal{L}_\lambda^A(\boldsymbol{n}) = \langle\boldsymbol{n}|\boldsymbol{u}\cdot\vec{\sigma}|\boldsymbol{n}\rangle = \boldsymbol{u}\cdot\boldsymbol{n},$$
$$\mathcal{L}_\lambda^B(\boldsymbol{m}) = \langle\boldsymbol{m}|\boldsymbol{v}\cdot\vec{\sigma}|\boldsymbol{m}\rangle = \boldsymbol{v}\cdot\boldsymbol{m}. \tag{A11}$$

Combining inequalities (A8) and (A11) and after an integration, one arrives at

$$\int\rho(\lambda)d\lambda\left|\mathcal{L}_\lambda^{AB}(\boldsymbol{n},\boldsymbol{m}) \pm \mathcal{L}_\lambda^{AB}(\boldsymbol{n},\boldsymbol{m}')\right| + \int\rho(\lambda)d\lambda|\boldsymbol{v}\cdot(\boldsymbol{m}\mp\boldsymbol{m}')| \leqslant 2. \tag{A12}$$

We consider three triplets of measurement settings $(\boldsymbol{n_1},\boldsymbol{m_1},\boldsymbol{m_1'})$, $(\boldsymbol{n_1},\boldsymbol{m_2},\boldsymbol{m_2'})$, and $(\boldsymbol{n_2},\boldsymbol{m_3},\boldsymbol{m_3'})$, as shown in Fig. 1 in the main text. The angle between $\boldsymbol{m}_i$ and $\boldsymbol{m}_i'$ ($i=1,2,3$) is ϕ, and $\boldsymbol{m_i}-\boldsymbol{m_i'} = 2\sin\frac{\phi}{2}\vec{e}_i$, where $\vec{e}_1,\vec{e}_2,\vec{e}_3$ form an orthogonal basis. Combining the fact that $\sum_i|\boldsymbol{v}\cdot\vec{e}_i| \geqslant 1$ and Eq. (A12), one obtains the Leggett-type inequality used in our experiment,

$$\mathcal{I}_{26}(\phi) = \left|C_{\boldsymbol{n_1},\boldsymbol{m_1}}+C_{\boldsymbol{n_1},\boldsymbol{m_1'}}\right| + \left|C_{\boldsymbol{n_1},\boldsymbol{m_2}}+C_{\boldsymbol{n_1},\boldsymbol{m_2'}}\right| + \left|C_{\boldsymbol{n_2},\boldsymbol{m_3}}+C_{\boldsymbol{n_2},\boldsymbol{m_3'}}\right| + 2\sin\frac{\phi}{2} \leqslant 6, \tag{A13}$$

where $C_{\boldsymbol{n},\boldsymbol{m}} = \sum_{\alpha,\beta}\alpha\beta P(\alpha,\beta|\boldsymbol{n},\boldsymbol{m})$ denotes the usual correlation function and ϕ is the angle depending on Bob's measurement settings. For two-qubit Bell states, we get the quantum expectation for $\mathcal{I}_{26}(\phi)$,

$$\mathcal{I}_{26}(\phi) = 6\left|\cos\frac{\phi}{2}\right| + 2\sin\frac{\phi}{2}. \tag{A14}$$

It is obvious from Eq. (A14) that Eq. (A13) can be violated by appropriately choosing ϕ, and the maximal violation is $\sqrt{40}$ occurring at $\phi = 2\arctan\frac{1}{3} \approx 36.9^\circ$.

Similar to the case of testing Bell inequalities, one may increase the number of measurement settings to obtain stronger quantum violations. In Eq. (A13), Alice has two measurement settings, whereas Bob has six settings. Following a similar derivation, one can obtain another Leggett-type inequality with more settings, but smaller critical visibility and fidelity:

$$\mathcal{I}_{28}(\varphi) = \left|C_{\boldsymbol{n_1},\boldsymbol{m_1}}+C_{\boldsymbol{n_1},\boldsymbol{m_1'}}\right| + \left|C_{\boldsymbol{n_1},\boldsymbol{m_2}}+C_{\boldsymbol{n_1},\boldsymbol{m_2'}}\right| + \left|C_{\boldsymbol{n_2},\boldsymbol{m_3}}+C_{\boldsymbol{n_2},\boldsymbol{m_3'}}\right| + \left|C_{\boldsymbol{n_2},\boldsymbol{m_4}}+C_{\boldsymbol{n_2},\boldsymbol{m_4'}}\right| + \frac{8}{\sqrt{6}}\sin\frac{\varphi}{2} \leqslant 8. \tag{A15}$$

Similarly, for two-qubit Bell states, we get the quantum expectation of $\mathcal{I}_{28}(\varphi)$,

$$\mathcal{I}_{28}(\varphi) = 8\left|\cos\frac{\varphi}{2}\right| + \frac{8}{\sqrt{6}}\sin\frac{\varphi}{2}, \tag{A16}$$

and Eq. (A15) can be violated by a wide range of φ, which is clearly observed in our experiments.

APPENDIX B: EXPERIMENTAL DETAILS

All experiments in this paper are performed on an electronic grade diamond (Element Six) with a natural abundance

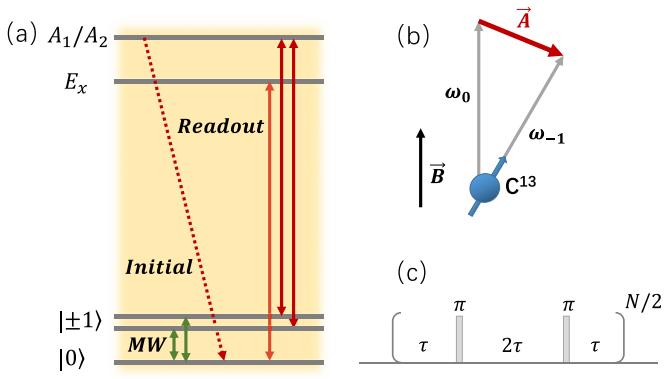

FIG. 5. (a) Illustration of energy levels of the NV center system, where resonant optical transitions between the ground and excited states are used for electron spin initialization and readout. The electron spin states are denoted by $|-1\rangle$ (dark state) and $|0\rangle$ (bright state), coherently manipulated by microwave fields. (b) Different axis nuclear-spin rotation while the electron spin state remains $|-1\rangle$ or $|0\rangle$ under the external magnetic field with each precession frequency, respectively. (c) Experimental dynamical decoupling (DD) sequences. Each microwave π pulse flips the electron spin state ($|-1\rangle \leftrightarrow |0\rangle$) with adjustable interpulse parameter τ.

of ^{13}C (1.1%) and a $\langle 100\rangle$ crystal orientation. We fabricate a solid-immersion lens (SIL) on the diamond sample to enhance the photoluminescence collection efficiency [56] and two surrounding gold striplines to apply resonant microwave fields. The chosen NV center has a natural ^{13}C nuclear-spin environment with hyperfine coupling strength A_{zz} varying from 5.50(7) to 564.3(3) kHz. We choose an appropriately coupled ^{13}C nuclear spin with the coupling strength $A_{zz} =$ 118.1(1) kHz as one of the qubits for this experiment to establish entanglement with the electron spin.

The sample is held in a commercial close-cycle cryostat (Nanoscale Workstation, Montana Instruments) at cryogenic temperature (~8 K). A permanent Samarium-Cobalt magnet outside the cryostat is used to apply the external magnetic field along NV axis with magnitude ~500 Gauss. For optical setup, two 637 nm lasers are used to initialize and read out the electron spin states, while one 532 nm laser is used to reset the NV center and keep it on the negative charge state. In experiments, all microwave fields are generated by a microwave source (Keysight N5181B) and an arbitrary-wave-form generator (AWG, Tektronix 5014C). Afterwards, we combine two microwave signals and transmit the signals through gold striplines into the cryostat.

In our experiments, we use individual optical transitions under appropriate selection rules to achieve single-shot readout and high-fidelity initialization of the NV electron spin [57]. After obtaining the corresponding frequency from photoluminescence excitation (PLE) spectroscopy to reconstruct energy levels of the NV center, we can prepare the electron spin in $|0\rangle$ by applying resonant pumping between $|\pm1\rangle \leftrightarrow |A_1/A_2\rangle$ [Fig. 5(a)]. The slight spin mixing within the excited states induces shelving into the other spin state, and high-fidelity spin-state initialization of more than $(99.0 \pm 0.1)\%$ [58] can be achieved through this optical pumping mechanism. Spin-dependent resonant transitions and low local strain (with strength ~1.0 GHz) also allow sufficient fidelity single-shot readout of the electron spin: we apply the $|0\rangle \leftrightarrow |E_x\rangle$ transition in experiment and use the presence or absence of fluorescence to distinguish the spin states. Due to the fabricated SIL on the sample, one or more photons are detected for the bright state ($|0\rangle$), while basically no photons are detected for the dark state ($|\pm1\rangle$) within the detection time.

TABLE I. Gate parameters of ^{13}C spin used in the experiments. Here, $R_{\pm X}^{\pi/2}$ denotes the nuclear-spin $\pi/2$ rotation around the x axis with a direction depending on the electron spin, while $R_Z^{\pi/2}$ denotes the nuclear-spin z-$\pi/2$ rotation.

U	τ (ns)	N	Gate duration (us)
$R_{\pm X}^{\pi/2}$	5450	28	306.04
$R_Z^{\pi/2}$	37	4	0.416

APPENDIX C: SYSTEM HAMILTONIAN CHARACTERIZATION

As described in the main text, we consider the system consisting of one electron spin and one weakly coupled ^{13}C nuclear spin. According to the conditioned evolution of nuclear spin based on the state of the electron spin state ($|-1\rangle$ or $|0\rangle$), the effective Hamiltonian in the main text can also be written as

$$H_{eff} = |1\rangle\langle 1| \otimes [(A_{zz} + \gamma_n B_z)\hat{I}_z + A_{zx}\hat{I}_x] + |0\rangle\langle 0| \otimes \gamma_n B_z \hat{I}_z. \tag{C1}$$

Here, $|0\rangle(|1\rangle)$ denotes the electron spin state $|0\rangle(|-1\rangle)$, respectively.

In this scheme, under the external magnetic field along the NV symmetry axis, nuclear spin undergoes precession of different frequency around the axis defined by the electron spin states [Fig. 5(b)]. For two electron spin states $|-1\rangle$ and $|0\rangle$, the nuclear spin evolves through different routes within the interpulse time τ. So, at specific τ condition, the final state of nuclear spin will be entangled with the electron spin in varying degrees. That forms the core internal mechanism of the dynamical decoupling (DD) sequence [Fig. 5(c)] [50]. For a weakly coupled ^{13}C spin environment, the corresponding parameter τ of the resonant condition reveals typical hyperfine coupling strength A_{zz}/A_{zx} through DD spectroscopy. Furthermore, we introduced an adaptive phase estimation algorithm to significantly improve the efficiency of learning the dominant Hamiltonian parameters with high precision in the previous experiments [49]. Experimentally, we choose a Carr-Purcell-Meiboom-Gill (CPMG) type of DD sequence and, after resolving the spin environment, we work with one ^{13}C nuclear spin of appropriate coupling strength [$A_{zz} = 118.1(1)$ kHz, $A_{zx} = 71(1)$ kHz]. Using the precisely calibrated parameters, we can finally design a set of electron-nuclear conditioned gates (Table I).

APPENDIX D: NUCLEAR-SPIN INITIALIZATION

As the beginning of experiments, we need to initialize nuclear spins in the system environment. First it comes to the measurement-based preparation on the strongly coupled nuclear spin, such as the host ^{14}N nuclear spin in our system. For

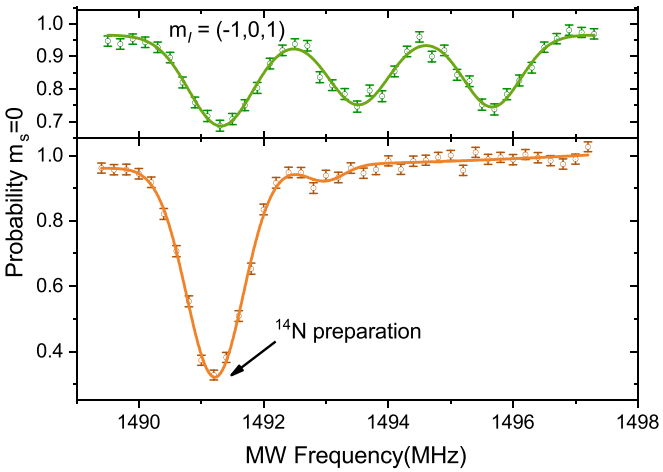

FIG. 6. The electron spin resonance experimental test before (green, top panel) and after (orange, bottom panel) polarizing the ^{14}N spin in the desired nuclear spin state. In the scheme, we repeat the initialization process twice to suppress imperfect optical detection errors and the corresponding single dip indicates the ^{14}N polarization in $|m_I = -1\rangle$.

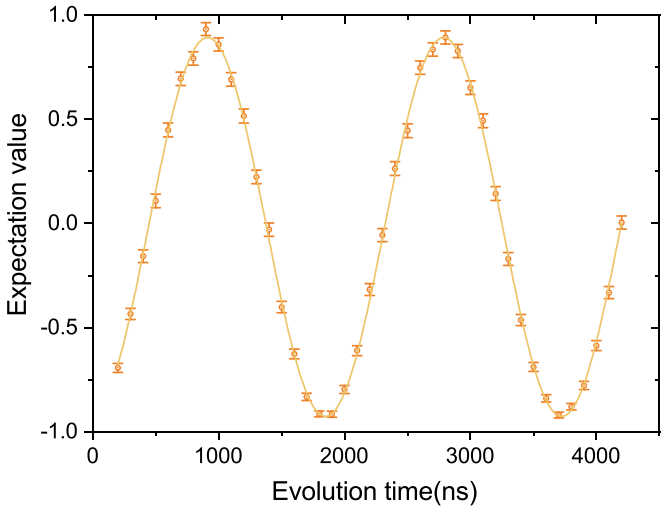

FIG. 7. ^{13}C nuclear-spin measurement results (dots) in the Y basis within free evolution time t after initialization, where the observed oscillation indicates the efficient control of the target nuclear spin. The cosinusoidal fitting result (solid line) demonstrates maximal readout-initialization combined fidelity of 0.96(1) with optimized gate parameters.

the previous experimental scheme [57], the procedure begins with preparing the electron spin in $|\pm 1\rangle$ states. However, the efficiency of ^{14}N polarization can be increased following the state-of-the-art NV technologies [59]: instead we choose to initialize the electron spin state into $|0\rangle$ and then apply a fast resonant microwave π pulse to drive $|0\rangle \leftrightarrow |-1\rangle$. Due to the high efficiency of this scheme, we can perform the initialization process twice to further improve the preparation fidelity of ^{14}N. Although it is extremely challenging to precisely measure the nuclear-spin polarization rate of ^{14}N [57], one can make sure that the rate is high enough for further experiments after an electron-spin resonance experimental test (Fig. 6).

The initialization of weakly coupled ^{13}C nuclear spin is composed of a swapping operation mapping electron spin onto the corresponding nuclear spin (see the main text). We also tune the gate parameters to obtain better state preparation: for the ^{13}C nuclear spin that is used, after state preparation, we optimize the single and controlled gate parameters, measuring free evolution in the Y basis (Fig. 7). In our experiments, we obtain initialization and readout combined fidelity with maximal value 0.96(1), and the same gate parameter set is used for the following experiments.

APPENDIX E: COMBINED READOUT OF ENTANGLED STATES

To test Leggett's inequalities, we design two sets of measurement settings, i.e., one for Eq. (2) and the other for Eq. (4) in the main text. For the combined readout of electron-nuclear entangled states in the corresponding basis $\varphi_e X_n/\varphi_e Y_n$, there are two cases for φ settings of the inclined angle between $(\boldsymbol{m_i}, \boldsymbol{m_i'})$ for Bob (electron spin), while in both cases $\boldsymbol{n_1}/\boldsymbol{n_2}$ is a unit vector along the X/Y direction for Alice (^{13}C nuclear spin), as shown in Figs. 1 and 4 in the main text. More precisely, for the six-setting case, the six measurement directions for Bob are as follows:

$$\begin{aligned}
\boldsymbol{m_1} &= \left(\cos\frac{\phi}{2}, 0, -\sin\frac{\phi}{2}\right), \quad \boldsymbol{m_1'} = \left(\cos\frac{\phi}{2}, 0, \sin\frac{\phi}{2}\right),\\
\boldsymbol{m_2} &= \left(\cos\frac{\phi}{2}, -\sin\frac{\phi}{2}, 0\right), \quad \boldsymbol{m_2'} = \left(\cos\frac{\phi}{2}, \sin\frac{\phi}{2}, 0\right),\\
\boldsymbol{m_3} &= \left(-\sin\frac{\phi}{2}, \cos\frac{\phi}{2}, 0\right), \quad \boldsymbol{m_3'} = \left(\sin\frac{\phi}{2}, \cos\frac{\phi}{2}, 0\right).
\end{aligned} \tag{E1}$$

Similarly, for the eight-setting case, the eight measurement directions for Bob are

$$\begin{aligned}
\boldsymbol{m_1} &= \left(\cos\frac{\varphi}{2}, -\frac{2}{\sqrt{6}}\sin\frac{\varphi}{2}, \frac{1}{\sqrt{3}}\sin\frac{\varphi}{2}\right),\\
\boldsymbol{m_1'} &= \left(\cos\frac{\varphi}{2}, \frac{2}{\sqrt{6}}\sin\frac{\varphi}{2}, -\frac{1}{\sqrt{3}}\sin\frac{\varphi}{2}\right),\\
\boldsymbol{m_2} &= \left(\cos\frac{\varphi}{2}, -\frac{2}{\sqrt{6}}\sin\frac{\varphi}{2}, -\frac{1}{\sqrt{3}}\sin\frac{\varphi}{2}\right),\\
\boldsymbol{m_2'} &= \left(\cos\frac{\varphi}{2}, \frac{2}{\sqrt{6}}\sin\frac{\varphi}{2}, \frac{1}{\sqrt{3}}\sin\frac{\varphi}{2}\right),\\
\boldsymbol{m_3} &= \left(-\frac{2}{\sqrt{6}}\sin\frac{\varphi}{2}, \cos\frac{\varphi}{2}, -\frac{1}{\sqrt{3}}\sin\frac{\varphi}{2}\right),\\
\boldsymbol{m_3'} &= \left(\frac{2}{\sqrt{6}}\sin\frac{\varphi}{2}, \cos\frac{\varphi}{2}, \frac{1}{\sqrt{3}}\sin\frac{\varphi}{2}\right),\\
\boldsymbol{m_4} &= \left(-\frac{2}{\sqrt{6}}\sin\frac{\varphi}{2}, \cos\frac{\varphi}{2}, \frac{1}{\sqrt{3}}\sin\frac{\varphi}{2}\right),\\
\boldsymbol{m_4'} &= \left(\frac{2}{\sqrt{6}}\sin\frac{\varphi}{2}, \cos\frac{\varphi}{2}, -\frac{1}{\sqrt{3}}\sin\frac{\varphi}{2}\right).
\end{aligned} \tag{E2}$$

To achieve the combined measurements, we need to rotate the electron spin ($\boldsymbol{m_i}$, $\boldsymbol{m_i'}$) to the X/Y axis. The whole process starts with a rotation to the Z axis and then a driving to the X/Y axis for the final readout, all controlled by the microwave fields through the modulation of output amplitude A, respective phase Ψ, and duration time T. For example, the expression of $\boldsymbol{m_i}$ can be rewritten as

$$\boldsymbol{m_i} = (\sin\Theta\cos\Phi, \sin\Theta\sin\Phi, \cos\Theta), \tag{E3}$$

where Θ denotes the zenith angle from the positive Z axis and Φ denotes the azimuth angle from the positive X axis, respectively. Experimentally, we rotate the electron spin along the axis $(\Phi - \pi/2)$ with angle Θ to return back to the positive Z axis and then projected into the X/Y axis by the corresponding $\pi/2$ microwave pulse.

After the projection of the electron spin, we subsequently use the designed sequence to achieve the joint detection X_eX_n/Y_eY_n of Alice (^{13}C nuclear spin) and Bob (electron spin) simultaneously to test Leggett's nonlocal model.

APPENDIX F: RAW-DATA VERIFICATION AND READOUT ERROR CORRECTION

For the two sets of experimentally observed correlations for testing Leggett's inequalities described in the main text, we now analyze the raw data without readout correction under normalization corresponding to the contrast in Rabi oscillation.

In both cases, we consider the error bars from readout standard deviations in stochastic state projection and optical measurement processes of a Bernoulli distribution, which is taken as the standard deviation in Monte Carlo methods,

$$\sigma = \sqrt{\frac{p_0(1-p_0)}{N}} \times F \times 2, \tag{F1}$$

where p_0 denotes the readout probability in $|0\rangle$, N is the repeating number of the measurement sequence, and F is the normalization factor corresponding to the contrast in Rabi oscillation; the factor of two in Eq. (F1) is due to the rescaling of measurement values from [0,1] to [−1, 1].

As for the raw-data verification, we include error bars for the two scenarios (six and eight settings) without data correction, shown in Figs. 3 and 4(b) in the main text. Notably, the maximal expectation values of two measurement settings are equal to 6.136 ± 0.034 and 8.323 ± 0.045, violating the corresponding Leggett's inequalities by more than 4.0 and 7.1 standard deviations, respectively.

For further data processing, we need to avoid the effect for infidelities during the measurement sequence and obtain the accurate value after entanglement preparation. The result is corrected based on the previous work [54]. For a single nuclear spin, we first prepare it into the eigenstate $|\downarrow\rangle$, then project it into the Y basis, and measure after the varied evolution time t. The spin preparation and projective readout operation consist of the same set of gates; thus, after appropriate fitting of the result, for a single nuclear spin, we assume that $C_{\text{initial}} = C_{\text{readout}} = C_Q$ and get the expressions

$$|\langle Y_+\rangle| = C_{Q+}^2, \tag{F2a}$$
$$|\langle Y_-\rangle| = C_{Q-}^2, \tag{F2b}$$

while $\langle Y_+\rangle$ and $\langle Y_-\rangle$ are the max and min cosinusoidal fitting value of the Y basis. After that, we can extract the factors $C_{Q+/-}$, which is associated with the measurement processes, and obtain the calibrated data in the main text.

[1] A. Einstein, B. Podolsky, and N. Rosen, Can quantum-mechanical description of physical reality be considered complete? Phys. Rev. **47**, 777 (1935).

[2] J. S. Bell, On the Einstein-Podolsky-Rosen paradox, Phys. Phys. Fiz. **1**, 195 (1964).

[3] N. Brunner, D. Cavalcanti, S. Pironio, V. Scarani, and S. Wehner, Bell nonlocality, Rev. Mod. Phys. **86**, 419 (2014).

[4] A. J. Leggett, Realism and the physical world, Rep. Prog. Phys. **71**, 022001 (2008).

[5] J. S. Bell and J. S. Bell, *Speakable and Unspeakable in Quantum Mechanics: Collected Papers on Quantum Philosophy* (Cambridge University Press, Cambridge, 2004).

[6] S. J. Freedman and J. F. Clauser, Experimental Test of Local Hidden-Variable Theories, Phys. Rev. Lett. **28**, 938 (1972).

[7] A. Aspect, J. Dalibard, and G. Roger, Experimental Test of Bell's Inequalities Using Time-Varying Analyzers, Phys. Rev. Lett. **49**, 1804 (1982).

[8] G. Weihs, T. Jennewein, C. Simon, H. Weinfurter, and A. Zeilinger, Violation of Bell's Inequality Under Strict Einstein Locality Conditions, Phys. Rev. Lett. **81**, 5039 (1998).

[9] M. A. Rowe, D. Kielpinski, V. Meyer, C. A. Sackett *et al.*, Experimental violation of a Bell's inequality with efficient detection, Nature (London) **409**, 791 (2001).

[10] M. Giustina, A. Mech, S. Ramelow, B. Wittmann, J. Kofler, J. Beyer, A. Lita, B. Calkins, T. Gerrits, S. W. Nam *et al.*, Bell violation using entangled photons without the fair-sampling assumption, Nature (London) **497**, 227 (2013).

[11] B. G. Christensen, K. T. McCusker, J. B. Altepeter, B. Calkins, T. Gerrits, A. E. Lita, A. Miller, L. K. Shalm, Y. Zhang, S. W. Nam, N. Brunner, C. C. W. Lim, N. Gisin, and P. G. Kwiat, Detection-Loophole-Free Test of Quantum Nonlocality, and Applications, Phys. Rev. Lett. **111**, 130406 (2013).

[12] M. Eibl, S. Gaertner, M. Bourennane, C. Kurtsiefer, M. Żukowski, and H. Weinfurter, Experimental Observation of Four-Photon Entanglement from Parametric Down-Conversion, Phys. Rev. Lett. **90**, 200403 (2003).

[13] Z. Zhao, T. Yang, Y.-A. Chen, A.-N. Zhang, M. Żukowski, and J.-W. Pan, Experimental Violation of Local Realism by Four-Photon Greenberger-Horne-Zeilinger Entanglement, Phys. Rev. Lett. **91**, 180401 (2003).

[14] B. P. Lanyon, M. Zwerger, P. Jurcevic, C. Hempel, W. Dür, H. J. Briegel, R. Blatt, and C. F. Roos, Experimental Violation of Multipartite Bell Inequalities with Trapped Ions, Phys. Rev. Lett. **112**, 100403 (2014).

[15] J. Hofmann, M. Krug, N. Ortegel, L. Gérard, M. Weber, W. Rosenfeld, and H. Weinfurter, Heralded entanglement

between widely separated atoms, Science **337**, 72 (2012).

[16] W. Pfaff, T. H. Taminiau, L. Robledo, H. Bernien, M. Markham, D. J. Twitchen, and R. Hanson, Demonstration of entanglement-by-measurement of solid-state qubits, Nat. Phys. **9**, 29 (2013).

[17] M. Ansmann, H. Wang, R. C. Bialczak, M. Hofheinz, E. Lucero, M. Neeley, A. O'connell, D. Sank, M. Weides, J. Wenner *et al.*, Violation of Bell's inequality in Josephson phase qubits, Nature (London) **461**, 504 (2009).

[18] C. Zu, D.-L. Deng, P.-Y. Hou, X.-Y. Chang, F. Wang, and L.-M. Duan, Experimental Distillation of Quantum Nonlocality, Phys. Rev. Lett. **111**, 050405 (2013).

[19] B. Hensen, H. Bernien, A. E. Dréau, A. Reiserer, N. Kalb, M. S. Blok, J. Ruitenberg, R. F. Vermeulen, R. N. Schouten, C. Abellán *et al.*, Loophole-free Bell inequality violation using electron spins separated by 1.3 kilometres, Nature (London) **526**, 682 (2015).

[20] M. Giustina, M. A. M. Versteegh, S. Wengerowsky, J. Handsteiner, A. Hochrainer, K. Phelan, F. Steinlechner, J. Kofler, J.-A. Larsson, C. Abellán, W. Amaya, V. Pruneri, M. W. Mitchell, J. Beyer, T. Gerrits, A. E. Lita, L. K. Shalm, S. W. Nam, T. Scheidl, R. Ursin, B. Wittmann, and A. Zeilinger, Significant-Loophole-Free Test of Bell's Theorem with Entangled Photons, Phys. Rev. Lett. **115**, 250401 (2015).

[21] L. K. Shalm, E. Meyer-Scott, B. G. Christensen, P. Bierhorst, M. A. Wayne, M. J. Stevens, T. Gerrits, S. Glancy, D. R. Hamel, M. S. Allman, K. J. Coakley, S. D. Dyer, C. Hodge, A. E. Lita, V. B. Verma, C. Lambrocco, E. Tortorici, A. L. Migdall, Y. Zhang, D. R. Kumor, W. H. Farr, F. Marsili, M. D. Shaw, J. A. Stern, C. Abellán, W. Amaya, V. Pruneri, T. Jennewein, M. W. Mitchell, P. G. Kwiat, J. C. Bienfang, R. P. Mirin, E. Knill, and S. W. Nam, Strong Loophole-Free Test of Local Realism, Phys. Rev. Lett. **115**, 250402 (2015).

[22] W. Rosenfeld, D. Burchardt, R. Garthoff, K. Redeker, N. Ortegel, M. Rau, and H. Weinfurter, Event-Ready Bell Test Using Entangled Atoms Simultaneously Closing Detection and Locality Loopholes, Phys. Rev. Lett. **119**, 010402 (2017).

[23] M. Genovese, Research on hidden variable theories: A review of recent progresses, Phys. Rep. **413**, 319 (2005).

[24] B. B. T. Collaboration *et al.*, Challenging local realism with human choices, Nature (London) **557**, 212 (2018).

[25] D. Bohm, A suggested interpretation of the quantum theory in terms of "hidden" variables. I, Phys. Rev. **85**, 166 (1952).

[26] A. Suarez and V. Scarani, Does entanglement depend on the timing of the impacts at the beam-splitters? Phys. Lett. A **232**, 9 (1997).

[27] H. Zbinden, J. Brendel, N. Gisin, and W. Tittel, Experimental test of nonlocal quantum correlation in relativistic configurations, Phys. Rev. A **63**, 022111 (2001).

[28] A. Stefanov, H. Zbinden, N. Gisin, and A. Suarez, Quantum Correlations with Spacelike Separated Beam Splitters in Motion: Experimental Test of Multisimultaneity, Phys. Rev. Lett. **88**, 120404 (2002).

[29] A. J. Leggett, Nonlocal hidden-variable theories and quantum mechanics: An incompatibility theorem, Found. Phys. **33**, 1469 (2003).

[30] S. Gröblacher, T. Paterek, R. Kaltenbaek, Č. Brukner, M. Żukowski, M. Aspelmeyer, and A. Zeilinger, An experimental test of non-local realism, Nature (London) **446**, 871 (2007).

[31] T. Paterek, A. Fedrizzi, S. Gröblacher, T. Jennewein, M. Żukowski, M. Aspelmeyer, and A. Zeilinger, Experimental Test of Nonlocal Realistic Theories Without the Rotational Symmetry Assumption, Phys. Rev. Lett. **99**, 210406 (2007).

[32] C. Branciard, A. Ling, N. Gisin, C. Kurtsiefer, A. Lamas-Linares, and V. Scarani, Experimental Falsification of Leggett's Nonlocal Variable Model, Phys. Rev. Lett. **99**, 210407 (2007).

[33] C. Branciard, N. Brunner, N. Gisin, C. Kurtsiefer, A. Lamas-Linares, A. Ling, and V. Scarani, Testing quantum correlations versus single-particle properties within Leggett's model and beyond, Nat. Phys. **4**, 681 (2008).

[34] M. Paternostro and H. Jeong, Testing nonlocal realism with entangled coherent states, Phys. Rev. A **81**, 032115 (2010).

[35] J. Romero, J. Leach, B. Jack, S. M. Barnett, M. J. Padgett, and S. Franke-Arnold, Violation of Leggett inequalities in orbital angular momentum subspaces, New J. Phys. **12**, 123007 (2010).

[36] C.-W. Lee, M. Paternostro, and H. Jeong, Faithful test of nonlocal realism with entangled coherent states, Phys. Rev. A **83**, 022102 (2011).

[37] F. Cardano, E. Karimi, L. Marrucci, C. de Lisio, and E. Santamato, Violation of Leggett-type inequalities in the spin-orbit degrees of freedom of a single photon, Phys. Rev. A **88**, 032101 (2013).

[38] Y. Hasegawa, C. Schmitzer, H. Bartosik, J. Klepp, S. Sponar, K. Durstberger-Rennhofer, and G. Badurek, Falsification of Leggett's model using neutron matter waves, New J. Phys. **14**, 023039 (2012).

[39] H.-Y. Su, J.-L. Chen, C. Wu, D.-L. Deng, and C. Oh, Testing Leggett's inequality using Aharonov-Casher effect, Sci. Rep. **3**, 2492 (2013).

[40] A. Suarez, Nonlocal "Realistic" Leggett models can be considered refuted by the before-before experiment, Found. Phys. **38**, 583 (2008).

[41] A. Rai, D. Home, and A. S. Majumdar, Leggett-type nonlocal realistic inequalities without any constraint on the geometrical alignment of measurement settings, Phys. Rev. A **84**, 052115 (2011).

[42] A. Sattar Khan, J.-L. Li, and C.-F. Qiao, Test of nonlocal hidden variable theory by the Leggett inequality in high energy physics, Phys. Rev. D **101**, 096016 (2020).

[43] S. Pironio, A. Acín, S. Massar, A. B. de La Giroday, D. N. Matsukevich, P. Maunz, S. Olmschenk, D. Hayes, L. Luo, T. A. Manning *et al.*, Random numbers certified by Bell's theorem, Nature (London) **464**, 1021 (2010).

[44] D.-L. Deng and L.-M. Duan, Fault-tolerant quantum random-number generator certified by Majorana fermions, Phys. Rev. A **88**, 012323 (2013).

[45] J. F. Clauser, M. A. Horne, A. Shimony, and R. A. Holt, Proposed Experiment to Test Local Hidden-Variable Theories, Phys. Rev. Lett. **23**, 880 (1969).

[46] M. W. Doherty, N. B. Manson, P. Delaney, F. Jelezko, J. Wrachtrup, and L. C. Hollenberg, The nitrogen-vacancy color center in diamond, Phys. Rep. **528**, 1 (2013).

[47] P. Neumann, Towards a room temperature solid state quantum processor-the nitrogen-vacancy center in diamond, Ph.D. thesis, University of Stuttgart, Germany, 2012.

[48] H. Bernien, Control, measurement and entanglement of remote quantum spin registers in diamond, Ph.D. thesis, Delft University of Technology, Netherlands, 2014.

[49] P.-Y. Hou, L. He, F. Wang, X.-Z. Huang, W.-G. Zhang, X.-L. Ouyang, X. Wang, W.-Q. Lian, X.-Y. Chang, and L.-M. Duan, Experimental Hamiltonian learning of an 11-qubit solid-state quantum spin register, Chin. Phys. Lett. **36**, 100303 (2019).

[50] T. H. Taminiau, J. J. T. Wagenaar, T. van der Sar, F. Jelezko, V. V. Dobrovitski, and R. Hanson, Detection and Control of Individual Nuclear Spins using a Weakly Coupled Electron Spin, Phys. Rev. Lett. **109**, 137602 (2012).

[51] A. Reiserer, N. Kalb, M. S. Blok, K. J. M. van Bemmelen, T. H. Taminiau, R. Hanson, D. J. Twitchen, and M. Markham, Robust Quantum-Network Memory using Decoherence-Protected Subspaces of Nuclear Spins, Phys. Rev. X **6**, 021040 (2016).

[52] T. H. Taminiau, J. Cramer, T. van der Sar, V. V. Dobrovitski, and R. Hanson, Universal control and error correction in multi-qubit spin registers in diamond, Nat. Nanotechnol. **9**, 171 (2014).

[53] G. Tóth and O. Gühne, Entanglement detection in the stabilizer formalism, Phys. Rev. A **72**, 022340 (2005).

[54] J. Cramer, N. Kalb, M. A. Rol, B. Hensen, M. S. Blok, M. Markham, D. J. Twitchen, R. Hanson, and T. H. Taminiau, Repeated quantum error correction on a continuously encoded qubit by real-time feedback, Nat. Commun. **7**, 11526 (2016).

[55] M. Ringbauer, C. Giarmatzi, R. Chaves, F. Costa, A. G. White, and A. Fedrizzi, Experimental test of nonlocal causality, Sci. Adv. **2**, 1600162 (2016).

[56] M. Jamali, I. Gerhardt, M. Rezai, K. Frenner, H. Fedder, and J. Wrachtrup, Microscopic diamond solid-immersion-lenses fabricated around single defect centers by focused ion beam milling, Rev. Sci. Instrum. **85**, 123703 (2014).

[57] L. Robledo, L. Childress, H. Bernien, B. Hensen, P. F. Alkemade, and R. Hanson, High-fidelity projective read-out of a solid-state spin quantum register, Nature (London) **477**, 574 (2011).

[58] P. Y. Hou, Experimental quantum information processing with diamond, Ph.D. thesis, Tsinghua University, China, 2018.

[59] C. E. Bradley, J. Randall, M. H. Abobeih, R. C. Berrevoets, M. J. Degen, M. A. Bakker, M. Markham, D. J. Twitchen, and T. H. Taminiau, A Ten-Qubit Solid-State Spin Register with Quantum Memory up to One Minute, Phys. Rev. X **9**, 031045 (2019).